

Discovery of a Metal-Line Absorber Associated with a Local Dwarf Starburst Galaxy

Brian A. Keeney¹, John T. Stocke¹, Jessica L. Rosenberg², Jason Tumlinson³,
and Donald G. York^{4,5}

ABSTRACT

We present optical and near-infrared images, H I 21 cm emission maps, optical spectroscopy, and *Hubble Space Telescope*/Space Telescope Imaging Spectrograph ultraviolet spectroscopy of the QSO/galaxy pair SBS 1122+594/IC 691. The QSO sight line lies at a position angle of 27° from the minor axis of the nearby dwarf starburst galaxy IC 691 ($cz_{\text{gal}} = 1204 \pm 3 \text{ km s}^{-1}$, $L_B \sim 0.09 L^*$, current star formation rate = $0.08\text{--}0.24 h_{70}^{-2} M_\odot \text{ yr}^{-1}$) and $33 h_{70}^{-1} \text{ kpc}$ ($6'.6$) from its nucleus. We find that IC 691 has an H I mass of $M_{\text{HI}} = (3.6 \pm 0.1) \times 10^8 M_\odot$ and a dynamical mass of $M_{\text{dyn}} = (3.1 \pm 0.5) \times 10^{10} h_{70}^{-1} M_\odot$. The UV spectrum of SBS 1122+594 shows a metal-line (Ly α +C IV) absorber near the redshift of IC 691 at $cz_{\text{abs}} = 1110 \pm 30 \text{ km s}^{-1}$. Since IC 691 is a dwarf starburst and the SBS 1122+594 sight line lies in the expected location for an outflowing wind, we propose that the best model for producing this metal-line absorber is a starburst wind from IC 691. We place consistent metallicity limits on IC 691 ($[Z/Z_\odot] \sim -0.7$) and the metal-line absorber ($[Z/Z_\odot] < -0.3$). We also find that the galaxy's escape velocity at the absorber location is $v_{\text{esc}} = 80 \pm 10 \text{ km s}^{-1}$ and derive a wind velocity of $v_w = 160 \pm 50 \text{ km s}^{-1}$. Thus, the evidence suggests that IC 691 produces an unbound starburst wind that escapes from its gravitational potential to transport metals and energy to the surrounding intergalactic medium.

¹Center for Astrophysics and Space Astronomy, Department of Astrophysical and Planetary Sciences, University of Colorado, 389 UCB, Boulder, CO 80309; keeney@casa.colorado.edu, stocke@casa.colorado.edu

²NSF Astronomy and Astrophysics Postdoctoral Fellow, Harvard-Smithsonian Center for Astrophysics, 60 Garden Street, Cambridge, MA 02138; jlrosenberg@cfa.harvard.edu

³Yale Center for Astronomy and Astrophysics, Departments of Physics and Astronomy, Yale University, New Haven, CT 06520; jason.tumlinson@yale.edu

⁴Department of Astronomy and Astrophysics, University of Chicago, 5640 South Ellis Avenue, Chicago, IL 60637

⁵Enrico Fermi Institute, University of Chicago, 5640 South Ellis Avenue, Chicago, IL 60637

Subject headings: galaxies: dwarf — galaxies: individual (IC 691) — galaxies: starburst — quasars: absorption lines — quasars: individual (SBS 1122+594)

1. Introduction

Metals have been distributed throughout much of the intergalactic medium (IGM) at all observed redshifts. Transport by galactic starburst winds is a leading theory for explaining the existence of these IGM metals, which are often found far (several hundred kiloparsecs; Stocke et al. 2006b) from any sites of ongoing star formation. However, it is not clear whether starbursts associated with luminous massive galaxies or smaller but more numerous dwarf galaxies produce the winds that are primarily responsible for enriching the IGM with metals and energy. Statistically, it appears that 0.1 L^* galaxies must contribute to IGM enrichment unless L^* galaxies can enrich regions up to ~ 1 Mpc in radius (Tumlinson & Fang 2005).

Starburst winds have been studied around nearby galaxies in emission using narrowband nebular emission line (e.g., $H\alpha$) and thermal X-ray continuum images (Watson, Stanger, & Griffiths 1984; Martin 1999; Martin, Kobulnicky, & Heckman 2002) as well as ultraviolet and optical absorption-line spectroscopy (Heckman et al. 2000, 2001; Rupke, Veilleux, & Sanders 2005a,b; Martin 2005, 2006; Keeney et al. 2005, 2006). Both imaging and absorption-line spectroscopy have limitations, but the two techniques are complementary in many ways. Emission-line studies can address the extent and morphology of the outflow, but only in its densest regions. These studies cannot measure the velocity or temperature of the outflow in the diffuse halo, so they are incapable of determining whether ejecta in the halo are bound to the galaxy. Thus, emission-line studies alone cannot determine which galaxies produce outflows that enrich the surrounding IGM. Absorption-line studies, on the other hand, are much more sensitive to diffuse gas and therefore can determine whether ejecta in the halo are bound to the galaxy, but only along one line of sight so they are unable to study the outflow morphology.

Most absorption-line studies also introduce an ambiguity in the distance between the background source and the absorbing gas since they typically use the stellar continuum of the starburst itself as their source (e.g., Heckman et al. 2000, 2001; Rupke et al. 2005a,b; Martin 2005, 2006). Consequently, they cannot distinguish a high-velocity outflow in the galactic halo from one in the starburst region itself. Using outflow velocities measured in the galactic disk to predict whether the absorbing gas is gravitationally bound to the galaxy is problematic because ejecta within several kiloparsecs of the starburst region will decelerate under the combined effects of gravity and mass loading (e.g., Suchkov et al. 1996; Martin et al. 2002; Strickland et al. 2004). This problem can be circumvented by probing the outflow

well away from the starburst region, which is only feasible if there is a bright background QSO projected near the galaxy of interest (e.g., Stocke et al. 2004; Keeney et al. 2005, 2006).

Massive galaxies have high rates of metal production and thus large amounts of potential fuel for IGM enrichment. Luminous low-redshift starbursts have star formation rates (SFRs) in the range $1\text{--}10 M_{\odot} \text{ yr}^{-1}$, although rates of $\sim 100\text{--}1000 M_{\odot} \text{ yr}^{-1}$ can be triggered by mergers (Heckman, Armus, & Miley 1990; Martin 2003; Rupke et al. 2005a,b). These galaxies generate winds with average outflow velocities of $300\text{--}400 \text{ km s}^{-1}$, but wind speeds of $\gtrsim 1000 \text{ km s}^{-1}$ are not unheard of (Heckman et al. 2000; Filippenko & Sargent 1992; Veilleux et al. 1994; Veilleux, Cecil, & Bland-Hawthorn 2005). Only the most luminous galaxies can be detected at high redshift, so studies of the earliest epochs of star formation and metal enrichment are inherently biased toward the most massive starbursts (Steidel et al. 1996a,b, 1999; Steidel, Pettini, & Adelberger 2001; Pettini et al. 2001, 2002; Adelberger et al. 2003).

Dwarf galaxies produce fewer metals per galaxy than their massive counterparts but they are much more numerous and their cumulative effects could dominate IGM enrichment (Stocke et al. 2004; Tumlinson & Fang 2005). Dwarf starburst galaxies have typical SFRs of $0.1\text{--}1 M_{\odot} \text{ yr}^{-1}$ (Martin 2003) and produce winds with outflow velocities of $\sim 50\text{--}200 \text{ km s}^{-1}$ (Marlowe et al. 1995; Martin 1998; Schwartz & Martin 2004). However, starbursts of all luminosities have the same maximum areal SFR ($\sim 45 M_{\odot} \text{ kpc}^{-2} \text{ yr}^{-1}$; Meurer et al. 1997) and produce winds with the same X-ray temperature (Martin 1999). These results indicate that dwarf starbursts may be more efficient than their massive counterparts at transporting the metals entrained in their winds to the IGM due to their shallower gravitational potentials with lower escape velocities.

Recent wind studies that utilize nearby QSOs to probe starburst winds several kiloparsecs from the host galaxy find that luminous galaxies produce bound winds while dwarf galaxies produce unbound winds. Keeney et al. (2005) found that the nearby luminous starburst galaxy NGC 3067 ($L \approx 0.5 L^*$, $\text{SFR} \approx 1.4 M_{\odot} \text{ yr}^{-1}$) produces a bound wind along the line of sight to 3C 232, which is located near the minor axis of NGC 3067 and $11 h_{70}^{-1} \text{ kpc}$ from the galactic plane. The Milky Way also produces a bound starburst wind along the lines of sight to two high-latitude AGN (Mrk 1383 and PKS 2005–489) at $l = 350^{\circ}$ that probe the regions on either side of the Galactic Center at heights up to 12.5 kpc (Keeney et al. 2006). On the other hand, Stocke et al. (2004) found that a dwarf poststarburst galaxy produced an unbound wind $\sim 3.5 \text{ Gyr}$ ago that is now observed as the 1586 km s^{-1} metal-line absorber in the spectrum of 3C 273, which is $71 h_{70}^{-1} \text{ kpc}$ away in projection on the sky.

In our on-going study to determine what type of galaxies enrich the IGM, this paper presents an ultraviolet spectrum of the QSO SBS 1122+594, as well as optical and near-infrared images, an H I 21 cm emission map, and an optical spectrum of the blue compact

galaxy IC 691, which is 6'6 away on the sky. These observations will be used to study whether the starburst wind produced by IC 691 can escape its gravitational potential to enrich the surrounding IGM. In §2 we describe the acquisition and reduction of our multi-wavelength observations. The connection between the metal-line absorber in the spectrum of SBS 1122+594 and IC 691 is discussed in §3. In §4 we examine whether the starburst wind produced by IC 691 can escape from its gravitational potential. We summarize our results and discuss their implications for IGM enrichment in §5.

2. Observations and Data Reduction

We have obtained images and spectra of the QSO/galaxy pair SBS 1122+594/IC 691 at several wavelengths. Our dataset includes ultraviolet and optical spectra of SBS 1122+594, as well as optical, near-infrared, and H I 21 cm images and a long-slit optical spectrum of IC 691. The acquisition and reduction of these data are described below in §§ 2.1–2.4. Broad-band optical images and fiber spectra of SBS 1122+594 and IC 691 are also available from the Sloan Digital Sky Survey (SDSS; York et al. 2000; Abazajian et al. 2005). SBS 1122+594 is located 6'6 from IC 691, which corresponds to an impact parameter of $33 h_{70}^{-1}$ kpc at the redshift of IC 691 assuming a distance of $cz_{\text{gal}}/H_0 = 17.2 h_{70}^{-1}$ Mpc ($cz_{\text{gal}} = 1204 \pm 3$ km s $^{-1}$; see §2.4).

2.1. Ultraviolet and Spectrum of SBS 1122+594

SBS 1122+594 was observed by the *Hubble Space Telescope* (HST) with the G140L grating of the Space Telescope Imaging Spectrograph (STIS) for 1320 seconds on 2004 Apr 6 as part of GO Program 9874 (PI: J. Tumlinson). Despite the short exposure time of this snapshot spectrum, an intergalactic Ly α +C IV absorber is evident near the redshift of IC 691. Figure 1 shows the associated Ly α and C IV absorption features, as well as an intergalactic Ly α line at $cz \approx 2350$ km s $^{-1}$ that can be seen in the upper panel. Information about other features in this spectrum, which covers wavelengths of ~ 1120 – 1720 Å, can be found in the Appendix.

The continuum near the associated Ly α and C IV absorption lines was normalized with Legendre polynomials and the Ly α and C IV features in the normalized spectra were fitted with Voigt profiles using a χ^2 minimization routine developed by B.A.K. Rest wavelengths, oscillator strengths, and transition rates for the Voigt profile fits were taken from Morton (2003). The fit to the C IV data was constrained such that both lines in the doublet

(rest wavelengths of 1548.2 and 1550.8 Å; Morton 2003) were fitted with the same velocity, Doppler b value, and ionic column density, resulting in a best fit with a velocity of $cz_{\text{abs}} = 1110 \pm 30 \text{ km s}^{-1}$ and a rest-frame equivalent width in the stronger, bluer line of $800 \pm 200 \text{ mÅ}$. The best-fit to the intergalactic Ly α absorber found a velocity of $1250 \pm 70 \text{ km s}^{-1}$ and a rest-frame equivalent width of $1700 \pm 200 \text{ mÅ}$. However, this absorber is located on the wing of the Galactic Ly α line and is further blended with another intergalactic Ly α absorber at $cz \approx 2350 \text{ km s}^{-1}$ at the low resolution of STIS with the G140L grating (see Fig. 1). We believe that this blending and the poorer resolution in the Ly α region ($\approx 430 \text{ km s}^{-1}$) as compared to the C IV region ($\approx 340 \text{ km s}^{-1}$) make the best-fit Ly α velocity untrustworthy. Therefore, we adopt the best-fit C IV velocity of $cz_{\text{abs}} = 1110 \pm 30 \text{ km s}^{-1}$ as the velocity of the Ly α +C IV absorber. This velocity is indicated by a vertical gray bar in Figure 1.

We have estimated the Ly α and C IV column densities for this absorber using the apparent optical depth (AOD) method (Savage & Sembach 1991). This method predicts a H I column density of $N_{\text{HI}} = 10^{14.6 \pm 0.1} \text{ cm}^{-2}$ for this absorber, which we treat as a lower limit to the true column density since the AOD method underpredicts the column density of saturated lines. Unresolved saturation is likely in this Ly α absorber due to the low velocity resolution of our G140L spectrum (e.g., the trough of the Galactic Ly α absorption feature in Fig. 1 is well above zero). Both lines of the C IV doublet yield AOD column densities that agree to within the combined errors. We adopt the column density predicted by the weaker line of the doublet, $N_{\text{CIV}} = 10^{14.7 \pm 0.2} \text{ cm}^{-2}$, since it is less susceptible to unresolved saturation. These column densities are used to estimate the absorber metallicity in §3.

2.2. Optical and Near-Infrared Images of IC 691

Broadband optical and H α images of IC 691 were obtained with the T2KA CCD at the Kitt Peak National Observatory (KPNO) 2.1-m telescope on 2003 Mar 4 and 2003 Mar 6. IC 691 was observed for a total exposure time of 480 s in B-band, 1680 s in R-band, and 2400 s each in the H α on- and off-band filters. A mosaic of R-band images showing both IC 691 and SBS 1122+594 is shown in Figure 2. Relative photometry with in-field standard stars yields an apparent B-band magnitude for IC 691, integrated to the 25th mag arcsec $^{-2}$ isophote ($r_{25} = 39'' = 3.3 h_{70}^{-1} \text{ kpc}$), of $m_{B,25} = 14.1 \pm 0.1$, which corresponds to an absolute magnitude of $M_B = -17.1 \pm 0.1$ and a luminosity of $L_B \approx 0.09 L^*$ (using M_B^* from Marzke, Huchra, & Geller 1994).

The inset to Figure 2 is a pure H α image of IC 691 and shows ongoing star formation in the nucleus of the galaxy. The stellar continuum was subtracted from our H α on-band image using a slightly bluer narrowband image. The resulting emission-line image of IC 691

contains flux not only from $H\alpha$, but also from the nearby [N II] 6548 Å line (the stronger [N II] 6584 Å line is redshifted out of our $H\alpha$ on-band filter). We have subtracted the [N II] flux from our emission-line image by assuming that the entire galaxy has a constant $F(H\alpha)/F([N II] 6548 \text{ \AA})$ ratio of 12, as found in our optical spectrum of IC 691 (see § 2.3 and Fig. 4). This pure $H\alpha$ image yields a total $H\alpha$ flux (corrected for Galactic extinction but not intrinsic extinction from IC 691) of $(2.9 \pm 0.1) \times 10^{-13} \text{ ergs s}^{-1} \text{ cm}^{-2}$ for IC 691, which corresponds to a $H\alpha$ luminosity of $(1.03 \pm 0.04) \times 10^{40} h_{70}^{-2} \text{ ergs s}^{-1}$ at the assumed distance to IC 691 of $17.2 h_{70}^{-1} \text{ Mpc}$. Using the conversion of Kennicutt (1998), this $H\alpha$ luminosity indicates a current SFR of $0.08 \pm 0.01 h_{70}^{-2} M_{\odot} \text{ yr}^{-1}$ for IC 691. After using the Balmer decrement in our optical spectrum of IC 691 (see § 2.3, Fig. 4, Table 1) to correct for the intrinsic extinction in IC 691, we find that its SFR is $0.24 \pm 0.03 h_{70}^{-2} M_{\odot} \text{ yr}^{-1}$. We treat this value as an upper limit on the SFR because we have most likely over-estimated the intrinsic extinction in IC 691 by applying an extinction correction derived from the densest region of the galaxy (i.e., the nuclear region where the Balmer decrement was measured) to our entire $H\alpha$ image. Thus, we have bounded the SFR of IC 691 to lie in the range $0.08\text{--}0.24 h_{70}^{-2} M_{\odot} \text{ yr}^{-1}$, which is comparable to the values of $0.1\text{--}1 M_{\odot} \text{ yr}^{-1}$ typically found in nearby dwarf starburst galaxies (Martin 2003).

Near-infrared H- and K-band images of IC 691 were obtained with the Near Infrared Camera (NIC) at the Apache Point Observatory ARC 3.5-m telescope on 2005 Apr 20. IC 691 was observed for a total exposure time of 100 s in both H- and K-band. We determined the surface brightness profile of the H-band images to find the photometric properties of the stellar distribution of IC 691 since the other broadband images were contaminated by nebular emission lines associated with star formation ([O II] in B-band, $H\alpha$ in R-band, and $Br\gamma$ in K-band). Figure 3 shows the H-band surface brightness profile of IC 691, generated with the IRAF tasks `ellipse` and `bmodel`, with a best-fit de Vaucouleurs (1948) $R^{1/4}$ profile overlaid. The dotted vertical line indicates the seeing of $0''.7$ in our image. Due to the small field of view of NIC there were no in-field standard stars, so the photometric zero point of $C_H = 23.93 \pm 0.03 \text{ mag}$ was determined by comparing the 2MASS H-band magnitudes of IC 691 at several apertures to the instrumental isophotal magnitudes at the same apertures. With this calibration, IC 691 has an H-band magnitude, integrated to the radius of the 20th mag arcsec $^{-2}$ K-band isophote ($r_{K20} = 13'' = 1.1 h_{70}^{-1} \text{ kpc}$), of $m_{H,K20} = 11.36 \pm 0.03$ and the best-fit $R^{1/4}$ profile has an effective radius of $r_e = 400 \pm 10 h_{70}^{-1} \text{ pc}$ and a fiducial surface brightness of $\mu_H(r_e) = 17.49 \pm 0.07 \text{ mag arcsec}^{-2}$. The ellipticity of the isophotes varies smoothly from $\epsilon = 0$ in the center of the galaxy to $\epsilon = 0.3$ at a semi-major axis of $1''.1$ ($\sim 90 h_{70}^{-1} \text{ pc}$) and stabilizes at this value for larger radii. Thus, IC 691 has an observed

axial ratio of 0.7 in H-band¹, implying that it is at an inclination of $i = 54^\circ \pm 2^\circ$ using the distribution of intrinsic dwarf galaxy shapes derived by Staveley-Smith, Davies, & Kinman (1992). Subtracting the model galaxy from our original H-band image reveals a residual stream of material to the north that we interpret as a tidal tail caused by an interaction with a nearby galaxy (see § 2.4).

2.3. Optical Spectrum of IC 691

An optical spectrum of IC 691 that covers 3600–9700 Å at ~ 6 Å resolution was obtained on 2003 May 2 with the Dual Imaging Spectrograph (DIS) at the Apache Point Observatory 3.5-m telescope. The spectrum is split onto two CCDs with reduced sensitivity from 5200–5600 Å due to a dichroic. The galaxy spectrum was acquired through a $1''.5$ slit rotated to a position angle of 90° and was extracted using a $12''$ wide aperture.

Table 1 lists the rest-frame equivalent widths for all emission lines detected in our optical spectrum of IC 691. This spectrum is displayed in Figure 4 with all emission lines from Table 1 labelled. The total H α flux in the spectrum is 2.3×10^{-13} ergs s⁻¹ cm⁻², or $\sim 80\%$ of the flux in the H α image (§ 2.2). The emission lines in Table 1 are observed at an average velocity of $\langle cz \rangle = 1200 \pm 30$ km s⁻¹, which agrees with the H I 21 cm velocity of $cz_{\text{gal}} = 1204 \pm 3$ km s⁻¹ found in § 2.4. We adopt the latter value as the best redshift of IC 691 due to its smaller error bars.

2.4. H I 21 cm Emission Map of IC 691

IC 691 was observed in the Very Large Array (VLA) D-array on 2003 Apr 23 with a bandwidth of 3.125 MHz centered at 1.422 GHz ($cz = 1200$ km s⁻¹) and a channel width of 48.8 kHz (10.4 km s⁻¹). The data were reduced using standard AIPS procedures: 3C 286 was used as a flux calibrator while 1035+564 (J2000) was used for the bandpass calibration. The data were then imaged using uniform weighting with the parameter ROBUST=0. After imaging, the data were continuum subtracted using IMLIN. In order to mask the noise in the cube before moment maps were constructed, the cube was first convolved with a Gaussian to a resolution of $100'' \times 100''$. This lower resolution cube was then blanked at the 2σ level

¹The SDSS images of IC 691 show that it has an axial ratio of ~ 0.6 in g' -, r' -, and i' -bands, which is consistent with the value implied by our R-band image. We adopt the H-band axial ratio of 0.7 because we believe that properties derived from the H-band images are more indicative of the general stellar population underlying the current starburst.

(1.8 mJy/beam) followed by blanking of the cube by hand to remove features that are not correlated from one channel to the next. This smoothed, blanked cube was then applied as a mask to the original data. The resultant cube was then used to create moment maps and spectra.

Figure 5 shows H I 21 cm intensity contours overlaid on a SDSS g' -band image of IC 691, which indicate that it is interacting with a low surface brightness (LSB) galaxy to the north, SDSS J112625.96+591737.5 (hereafter SDSS J1126+593). The SDSS spectrum of the LSB galaxy shows no emission lines and places it at a redshift of $cz = 1340 \pm 50 \text{ km s}^{-1}$. Interestingly, if we separate the H I 21 cm emission from IC 691 and SDSS J1126+593 by placing a cut at a declination of $59^\circ 14'$ we find a much lower redshift for SDSS J1126+593 of $cz = 1180 \pm 20 \text{ km s}^{-1}$. This same cut indicates that the H I 21 cm emission from SDSS J1126+593 has a FWHM of $26 \pm 6 \text{ km s}^{-1}$ and a H I mass of $M_{\text{HI}} = (4.6 \pm 0.5) \times 10^7 M_\odot$ and the H I around IC 691 has a velocity of $cz_{\text{gal}} = 1204 \pm 3 \text{ km s}^{-1}$, a FWHM of $116 \pm 3 \text{ km s}^{-1}$, and an H I mass of $M_{\text{HI}} = (3.6 \pm 0.1) \times 10^8 M_\odot$.

A tilted ring model was fit to the H I 21 cm velocity profile of IC 691, with the ring inclination fixed at the value ($i = 54^\circ$) predicted by the axial ratio of the optical and near-infrared images (§ 2.2). The approaching (northern) and receding (southern) sides of the galaxy were fit separately to search for evidence of tidal effects and agree to within errors for radii $< 14.2 h_{70}^{-1} \text{ kpc}$ ($170''$). At larger radii the two sides of the galaxy become more and more discrepant, indicating that tidal effects are becoming increasingly important. Our B-band images of IC 691 (§ 2.2) indicate that its Holmberg radius is $66'' = 5.5 h_{70}^{-1} \text{ kpc}$, so our $14.2 h_{70}^{-1} \text{ kpc}$ cutoff corresponds to a radius of ~ 2.5 Holmberg radii. Figure 6 shows our final rotation curve for IC 691, which was fit to both the approaching and receding sides of the galaxy simultaneously with a fixed inclination of $i = 54^\circ$ and is truncated at a radius of $14.2 h_{70}^{-1} \text{ kpc}$. This rotation curve is used to derive the dynamical mass of IC 691 in § 4.1.

3. Galaxy/Absorber Connection

Statistically, low column density ($N_{\text{HI}} \lesssim 10^{17.3} \text{ cm}^{-2}$) intergalactic Ly α absorbers are associated with overdense IGM filaments rather than individual luminous ($L > 0.1 L^*$) galaxies (Morris et al. 1993; Tripp, Lu, & Savage 1998; Impey, Petry, & Flint 1999; Penton, Stocke, & Shull 2002, 2004). Existing HST and FUSE spectra of QSO sight lines with low redshift intergalactic Ly α absorbers are not generally sensitive enough to detect metals (C II, C III, C IV, Si II, Si III, Si IV, O VI) in these absorbers except at $N_{\text{HI}} \gtrsim 10^{14} \text{ cm}^{-2}$ (Stocke, Shull, & Penton 2006a) where metallicities of 5–10% solar are found (Sembach et al. 2001; Tripp et al. 2002; Shull et al. 1998; Shull, Tumlinson, & Giroux 2003; Tumlinson

et al. 2005; Danforth & Shull 2005; Danforth et al. 2006, but see Aracil et al. 2006 and Prochaska et al. 2004 for individual absorber metallicities that may approach solar values). Weak metal-line systems are found to have smaller impact parameters from nearby galaxies than typical Ly α absorbers without associated metal lines (e.g., Stocke et al. 2006b) and the average QSO/galaxy impact parameter decreases with increasing column density. Thus, Damped Ly α Absorbers (DLAs), the highest column density systems ($N_{\text{HI}} > 10^{20.3} \text{ cm}^{-2}$), are plausibly associated with galactic disks (although see York et al. 2006 for a different hypothesis) and Lyman limit systems (LLSs; $N_{\text{HI}} = 10^{17.3-20.3} \text{ cm}^{-2}$) are likely associated with galactic halos (e.g., Steidel 1995, 1998), whereas lower column density metal-line absorbers ($N_{\text{HI}} = 10^{14-17.3} \text{ cm}^{-2}$) could be associated with outflowing galactic winds (see, e.g., Stocke et al. 2004, 2006a,b). These statistical results suggest that the Ly α +C IV absorber at $cz_{\text{abs}} = 1110 \pm 30 \text{ km s}^{-1}$ in the spectrum of SBS 1122+594 could be associated with a nearby galaxy.

Figure 7 shows the positions of all galaxies with $cz < 1600 \text{ km s}^{-1}$ that are within $500 h_{70}^{-1} \text{ kpc}$ of SBS 1122+594 ($100'$ at $cz = 1200 \text{ km s}^{-1}$), as compiled by SDSS and the NASA/IPAC Extragalactic Database (NED). The position of SBS 1122+594 is indicated by the filled star symbol in the center of the plot. The circular symbols represent galaxies with $cz < 1300 \text{ km s}^{-1}$ and the diamonds represent galaxies with $cz = 1300\text{--}1600 \text{ km s}^{-1}$. Symbol size is proportional to the SDSS r' -band luminosity of the galaxy. While no obvious groups of galaxies are evident, there is a large-scale “filament” of galaxies present in Figure 7 in which both IC 691 and the absorber are embedded. This absorber environment is similar to the filamentary environments of the 1586 km s^{-1} absorber towards 3C 273 and the 1685 km s^{-1} absorber towards RX J1230.8+0115 studied previously by Stocke et al. (2004) and Rosenberg et al. (2003). Any galaxies with unknown redshifts near SBS 1122+594 are fainter than the SDSS spectroscopic completeness limit of $m_r = 17.8$. At $cz_{\text{gal}} \approx cz_{\text{abs}}$, this limit implies that Figure 7 is complete to an absolute magnitude of $M_r - 5 \log h_{70} \leq -13.2$, or $L_r \geq 0.001 h_{70}^{-2} L^*$ (Blanton et al. 2001).

With impact parameters of $33 h_{70}^{-1} \text{ kpc}$ and $42 h_{70}^{-1} \text{ kpc}$, respectively, IC 691 and SDSS J1126+593 are by far the closest galaxies in Figure 7 to the SBS 1122+594 sight line. While the redshift of SDSS J1126+593 as derived from the centroid of its H I 21 cm emission is marginally closer to the absorber velocity than that of IC 691, IC 691 is ~ 20 times more luminous in SDSS r' -band than SDSS J1126+593. This luminosity difference, combined with the facts that IC 691 is currently forming stars while SDSS J1126+593 is not and IC 691 is closer to the SBS 1122+594 sight line, indicate that IC 691 is more likely to have created the metal-line absorber.

The closest luminous galaxy to SBS 1122+594 is NGC 3642 at $cz_{\text{gal}} = 1598 \text{ km s}^{-1}$,

which is $130 h_{70}^{-1}$ kpc away ($28'.3$ at cz_{abs}) and ~ 10 times more luminous than IC 691. We consider IC 691 to be the more likely source of the metal-line absorber, however, since NGC 3642 is both 4 times further from SBS 1122+594 in projection and 5 times more discrepant in redshift. Other than NGC 3642, the only galaxies in Figure 7 that are more luminous than IC 691 are NGC 3795B and NGC 3619, which are $452 h_{70}^{-1}$ kpc ($97'.9$ at cz_{abs}) and $458 h_{70}^{-1}$ kpc ($99'.2$ at cz_{abs}) away from SBS 1122+594, respectively. NGC 3795B is at a redshift of $cz = 1257 \text{ km s}^{-1}$ and is twice as luminous as IC 691, and NGC 3619 is at a redshift of $cz = 1553 \text{ km s}^{-1}$ and is ~ 6 times more luminous than IC 691. Neither of these galaxies are as luminous as NGC 3642 nor as close to the SBS 1122+594 sight line so they are not likely candidates for the origin of the metal-line absorber.

Several circumstantial lines of reasoning also point to a connection between IC 691 and the metal-line absorber. The $33 h_{70}^{-1}$ kpc impact parameter between SBS 1122+594 and IC 691 is much less than the median nearest-neighbor distance of $180 h_{70}^{-1}$ kpc between low-metallicity ($10 \pm 5\%$ solar) O VI and C III absorbers detected with FUSE and galaxies of any luminosity detected in regions where galaxy surveys are complete to at least $0.1 L^*$ (Stocke et al. 2006b). The SBS 1122+594 sight line also lies at a position angle $\theta = 27^\circ$ from the minor axis of IC 691, which is the expected direction for an outflowing starburst wind since nearby starburst galaxies often show biconic outflows with opening angles above the disk of $2\theta \approx 45^\circ\text{--}100^\circ$ (values of $2\theta \sim 65^\circ$ are typical; Heckman et al. 1990; Veilleux et al. 2005). Furthermore, the H I 21 cm emission along the major axis of IC 691 extends to distances comparable to the SBS 1122+594/IC 691 separation (see Fig. 5). While some of this material is affected by tidal interactions between IC 691 and SDSS J1126+593, the large extent of the H I envelope of IC 691 with respect to the angular distance between IC 691 and SBS 1122+594 indicates that gas associated with IC 691 can plausibly reach the location of SBS 1122+594 on the sky.

The H I emission map in Figure 5 suggests that the metal-line absorber could be due to the recent interaction between IC 691 and SDSS J1126+593. However, the extended H I is in a plane nearly perpendicular to the direction of SBS 1122+594 from IC 691, and while tidal tails are often strongly curved (e.g., NGC 520; Hibbard & van Gorkom 1996; Norman et al. 1996) the H I 21 cm emission of IC 691 shows no evidence of such curvature. Also, the H I velocities of the tidal border between these two galaxies is never less than $1180 \pm 20 \text{ km s}^{-1}$ at any location. Therefore, any tidal debris in the direction of SBS 1122+594 must be more diffuse and/or more highly-ionized and have different kinematics than the tidal material seen in Figure 5. The absence of velocity overlap between the H I tidal debris and the absorber argue against a tidal origin for the absorbing gas. So, while we cannot rule out tidal debris as the origin of the metal-line absorber, we believe that the outflowing gas from a starburst superwind triggered by the recent interaction is more likely. This model naturally

explains why absorption is seen near the minor axis of IC 691, which is far from the plane of the galaxy interaction (although outflows from dwarf galaxies may have less of a preferred direction than in more massive starbursts; e.g., Ott, Martin, & Walter 2003).

Table 1 lists the rest-frame equivalent widths for the emission lines detected in the IC 691 starburst with our optical spectrum (§ 2.3). The [O III] derived mean temperature of $\sim 14,000^\circ$ K is uncertain due to the weakness of the [O III] 4363 Å line in our spectrum, but is similar to [O III] derived temperatures for hotter H II regions in the LMC (Oey & Shields 2000). Likewise the relatively reddening-free line ratios [O III 5007 Å]/H β and [N II 6584 Å]/H α in IC 691 are also similar to values found for LMC H II regions by Oey et al. (2000). Because the Balmer decrement listed in Table 1 is only slightly larger than case-B, there is only quite modest reddening present in the H II region spectrum of IC 691 and should not effect these line ratios significantly. Since the detailed position-resolved abundance study of LMC H II regions by Oey & Shields (2000) found oxygen and nitrogen abundances of 20–30% solar, the mean metal abundances in the IC 691 starburst are comparable to those values based upon our long-slit spectrum. Therefore, the metal abundance in this dwarf starburst is significantly subsolar as expected for such a small galaxy.

Our STIS spectrum of SBS 1122+594 (see § 2.1 and Fig. 1) limits the H I and C IV column densities to $N_{\text{HI}} \geq 10^{14.6} \text{ cm}^{-2}$ and $N_{\text{CIV}} = 10^{14.7 \pm 0.2} \text{ cm}^{-2}$, respectively. A standard photoionization model can be employed to estimate the metallicity of this absorber by assuming an extragalactic photoionizing flux of $I_\nu = 10^{-23} \text{ ergs cm}^{-2} \text{ s}^{-1} \text{ Hz}^{-1}$ and a gas overdensity for this absorber of 10–100 based upon estimates from numerical simulations for the observed N_{HI} lower limit (i.e., $\log U = -0.5$ to -1.5). In this case the C IV equivalent width of 800 mÅ yields $[Z/Z_\odot] < -0.3$ and a particle density of $\sim 10^{-5} \text{ cm}^{-3}$, implying a scale-size along the line-of-sight (LOS) of $> 10 \text{ pc}$. It is quite unlikely that this absorber is either hotter, collisionally-ionized gas or diffuse photoionized gas because of the strength of the C IV absorption; however, searches for O VI in the far-UV and lower ions in the HST band should be conducted if better UV spectra become available to discriminate between these two possibilities. Our estimated absorber metallicity is broadly consistent with our metallicity estimate of $[Z/Z_\odot] \sim -0.7$ for IC 691, although the absorber metallicity could be less than that of IC 691 since there is only a lower limit on the absorber N_{HI} . However, the upper limit on the absorber metallicity is still significantly subsolar as expected from an outflow associated with a dwarf galaxy.

While the inferred LOS size for this absorber may seem quite small, it is comparable to the LOS scale-size for the 1586 km s $^{-1}$ absorber in the 3C 273 sightline (Tripp et al. 2002), as well as many “weak-Mg II” absorbers studied by Charlton et al. (2002) at higher redshifts. Stocke et al. (2004) argued that the small LOS sizes reported for weak metal-

line absorbers coupled with their relative frequency (which requires a scale-size on the sky of ~ 100 kpc) were naturally explained by the thin-shell geometry produced by a galactic superwind. Recent hydrodynamical simulations of dense clouds entrained in an outflowing galactic superwind by Marcolini et al. (2005) modelled these clouds as spheres with a radius of 15 pc, which is comparable to the LOS sizes of the 3C 273 and SBS 1122+594 absorbers discussed above. Therefore, both the subsolar metallicity of the metal-line absorber and its small size are suggestive of an origin in a dwarf galaxy superwind from IC 691.

4. Does the Starburst Wind Escape?

In this Section, we assume that the Ly α +C IV absorber in SBS 1122+594 is gas entrained in a starburst superwind from IC 691. Since galactic winds are a leading mechanism for transporting metals and energy from galaxies into the IGM, we use the Ly α +C IV absorber in SBS 1122+594 to determine whether the starburst wind from IC 691 can escape from its gravitational potential to enrich large regions of intergalactic space. The total mass of IC 691 is calculated in §4.1. In §4.2 we use this mass to derive various properties of the starburst wind.

4.1. Total Mass of IC 691

The H I 21 cm rotation curve discussed in §2.4 is shown in Figure 6. These data are truncated at a radius of $14.2 h_{70}^{-1}$ kpc ($170''$) because the interaction of IC 691 with SDSS J1126+593 (the LSB galaxy to the north; see Fig. 5) precludes us from extending the rotation curve to larger radii. However, the last data point in Figure 6 suggests that the H I 21 cm rotation curve has begun to flatten at radii $> 9.2 h_{70}^{-1}$ kpc ($110''$). In order to estimate the total mass of IC 691, we have assumed that the rotation curve has flattened at these radii and remains flat to a radius of $24.6 h_{70}^{-1}$ kpc ($295''$; ~ 4.5 Holmberg radii), the maximum radial extent of IC 691 (using the cut at a declination of $59^{\circ}14'$ to separate the H I emission from IC 691 and SDSS J1126+593; see §2.4). Under this assumption, the rotation curve was fit with an isothermal halo truncated at $24.6 h_{70}^{-1}$ kpc. The best-fit model (reduced $\chi^2 = 1.0$) is overlaid on the data points in Figure 6 and has a central density of $0.005 \pm 0.002 M_{\odot} \text{pc}^{-3}$ and a core radius of $6 \pm 2 h_{70}^{-1}$ kpc. The escape velocity as a function of radius predicted by the best-fit model is shown in Figure 6 by the solid line above the data points, and the point with the open triangle symbol indicates the observed wind velocity and absorber location. These quantities are discussed further in §4.2.

Assuming that the rotation curve of IC 691 is flat at a velocity of $74 \pm 9 \text{ km s}^{-1}$ to a radius of $24.6 h_{70}^{-1} \text{ kpc}$ and declines thereafter implies that IC 691 has a total mass of $M_{\text{dyn}} = (3.1 \pm 0.5) \times 10^{10} h_{70}^{-1} M_{\odot}$. This dynamical mass predicts a total mass-to-light ratio of $M_{\text{dyn}}/L_B = 28 \pm 5 h_{70}$ and a gas mass fraction of $f_{\text{gas}} \equiv M_{\text{HI}}/M_{\text{dyn}} = 0.012 \pm 0.002 h_{70}$ for IC 691. These values are consistent with the mass-to-light ratios and gas mass fractions found for nearby blue compact galaxies and dwarf irregular galaxies (Begum et al. 2005; Pisano et al. 2001; Roberts & Haynes 1994).

It is quite possible that this dynamical mass is an overestimate. Figure 5 shows that IC 691 is interacting with a nearby galaxy to the north, which should act to increase the turbulent motions in IC 691, and thus its velocity dispersion. Therefore, one would expect that only part of the velocity in Figure 6 is caused by galactic rotation with the remainder caused by the interaction. If this is correct it implies that the true dynamical mass of IC 691 is lower than our estimate. IC 691 is also well-fit by a de Vaucouleurs (1948) $R^{1/4}$ profile (Fig. 3), making it photometrically similar to elliptical galaxies rather than spirals, further implying that it may not be dominated by rotation. However, since our dynamical mass estimate of $M_{\text{dyn}} = (3.1 \pm 0.5) \times 10^{10} h_{70}^{-1} M_{\odot}$ predicts a mass-to-light ratio and gas mass fraction for IC 691 that are consistent with the range of values found for similar nearby galaxies, we will assume that it is valid for all subsequent calculations.

4.2. Starburst Wind Properties

We assume that the Ly α +C IV absorber is entrained in a radial outflow emanating from the galactic center of IC 691, that the galaxy’s mass distribution is spherically symmetric, and that all of the mass is located interior to the SBS 1122+594 sight line. Under these assumptions, IC 691 can be treated as a point-mass when calculating the escape velocity at the absorber location:

$$v_{\text{esc}} = 93 \text{ km s}^{-1} \left(\frac{M_{\text{dyn}}}{10^9 M_{\odot}} \right)^{1/2} \left(\frac{r}{\text{kpc}} \right)^{-1/2} \quad (1)$$

If IC 691 is at an inclination i then $M_{\text{dyn}} = ([2.0 \pm 0.3] \times 10^{10} h_{70}^{-1} M_{\odot}) / \sin^2 i$ (which corresponds to the value from §4.1 for $i = 54^\circ$), $r = (33 h_{70}^{-1} \text{ kpc}) / \sin i$, and $v_{\text{esc}} = (72 \pm 8 \text{ km s}^{-1}) / \sqrt{\sin i}$. The starburst wind has a LOS velocity of $v_{\text{los}} \equiv |cz_{\text{abs}} - cz_{\text{gal}}| = 95 \pm 30 \text{ km s}^{-1}$ at the absorber location, which corresponds to an outflow speed perpendicular to the disk of IC 691 of $v_w = v_{\text{los}} / \cos i$. The wind will escape the gravitational potential of IC 691 if $v_w / v_{\text{esc}} > 1$, which will occur at inclinations of $i > 26^\circ \pm 10^\circ$. The H-band axial ratio (§2.2) predicts an inclination of $i = 54^\circ \pm 2^\circ$ for IC 691. Thus, under our set of assumptions, IC 691 produces an unbound starburst wind.

With our assumed geometry and a galaxy inclination of $i = 54^\circ$, the escape velocity at the absorber location of $r = (33 h_{70}^{-1} \text{ kpc}) / \sin i = 41 h_{70}^{-1} \text{ kpc}$ is $v_{\text{esc}} = (72 \pm 8 \text{ km s}^{-1}) / \sqrt{\sin i} = 80 \pm 10 \text{ km s}^{-1}$ and the starburst wind is moving at a speed of $v_w = v_{\text{los}} / \cos i = 160 \pm 50 \text{ km s}^{-1}$. This outflow velocity places an upper limit on the time since the absorbing gas was ejected of $\tau_{\text{ej}} = r/v_w = 250 \pm 80 h_{70}^{-1} \text{ Myr}$, assuming that the wind has been moving at a constant velocity. This timescale is an upper limit since the ejecta would likely decelerate due to gravity and mass loading, and indicates that the metal-line absorber is associated with the current star formation episode in IC 691 or a burst immediately preceding it.

It is interesting to consider how much mass the current burst in IC 691 could eject as wind material. If the burst that created the metal-line absorber lasted for 10^8 years at the current SFR of IC 691 (uncorrected for intrinsic extinction), then $\sim 8 \times 10^6 M_\odot$ of stars were formed. A Salpeter initial mass function predicts that a burst of this size would create $\sim 10^5$ stars with $M > 8 M_\odot$, each of which would eventually become a supernova. If each supernova has 10^{51} ergs of energy available, which is converted to bulk motions with an efficiency of 3–30% (Cioffi & Shull 1991; Koo & McKee 1992a,b), then the burst produced $3 \times 10^{54-55}$ ergs that could be used to generate a wind. This energy can accelerate up to $6 \times 10^{6-7} M_\odot$ of material to a velocity of $\sim 160 \text{ km s}^{-1}$ after escaping the gravitational potential well of IC 691. Thus, the production of the metal-line absorber towards SBS 1122+594 by the IC 691 starburst is plausible energetically.

If IC 691 continues to form stars at its current rate of $0.08 \pm 0.01 h_{70}^{-2} M_\odot \text{ yr}^{-1}$ then it will run out of available material for additional star formation in the gas depletion timescale of $\tau_{\text{gas}} \equiv M_{\text{HI}}/\text{SFR} = 4.5 \pm 0.6 h_{70}^2 \text{ Gyr}$ (Kennicutt 1983). This timescale is longer than the duration of a typical star formation episode, so IC 691 will likely experience further star formation episodes once the current burst ceases. Complicated, episodic star formation histories are not uncommon for dwarf starbursts, as evidenced by the Local Group dwarf elliptical and spheroidal galaxies (Mateo 1998).

5. Conclusions

We have used HST to detect Ly α and C IV absorption ($cz_{\text{abs}} = 1110 \pm 30 \text{ km s}^{-1}$) from the nearby dwarf starburst galaxy IC 691 ($cz_{\text{gal}} = 1204 \pm 3 \text{ km s}^{-1}$) in the spectrum of the QSO SBS 1122+594. Narrowband H α images show that IC 691 is currently forming stars at a rate of $0.08\text{--}0.24 h_{70}^{-2} M_\odot \text{ yr}^{-1}$, which is comparable to the SFRs found in other nearby dwarf starburst galaxies (Martin 2003). A long-slit optical spectrum of IC 691 reveals H β , H γ , [O II], [O III], [N II], and [S II] emission in addition to H α . The H-band surface brightness profile of IC 691 is well-fit by a de Vaucouleurs (1948) $R^{1/4}$ profile, making it

photometrically similar to elliptical galaxies despite its current starburst. An H I 21 cm emission map obtained with the VLA shows that IC 691 is interacting with SDSS J1126+593, a LSB galaxy to the north (see Fig. 5), which could have triggered its current epoch of star formation. Eliminating as much tidal material as possible by-eye, IC 691 has a H I mass of $M_{\text{HI}} = (3.6 \pm 0.1) \times 10^8 M_{\odot}$ and its H I 21 cm rotation curve (Fig. 6) implies that it has a dynamical mass of $M_{\text{dyn}} = (3.1 \pm 0.5) \times 10^{10} h_{70}^{-1} M_{\odot}$.

Since IC 691 is a dwarf starburst galaxy and the SBS 1122+594 sight line lies in the expected direction of a starburst wind (Heckman et al. 1990; Veilleux et al. 2005), we suggest that the metal-line absorber at $cz_{\text{abs}} = 1110 \pm 30 \text{ km s}^{-1}$ is caused by an outflowing starburst wind from IC 691. If this is indeed the case, then the wind produced by IC 691 will escape its gravitational potential to enrich the surrounding IGM since the escape velocity at the absorber location is $v_{\text{esc}} = 80 \pm 10 \text{ km s}^{-1}$ and the wind velocity is $v_w = 160 \pm 50 \text{ km s}^{-1}$. If the absorbing gas was ejected from IC 691 when it was forming stars at its current rate in a burst lasting $\sim 10^8$ years, then it could accelerate $\gtrsim 10^7 M_{\odot}$ of material to the current absorber velocity. A rough estimate of a subsolar metallicity ($[Z/Z_{\odot}] < -0.3$) for this absorber is also consistent with the metallicity limit of $[Z/Z_{\odot}] \sim -0.7$ found for IC 691.

Our conclusion that IC 691 produces an unbound starburst wind agrees with the results of Stocke et al. (2004), who found that an unbound wind from a dwarf poststarburst galaxy could be responsible for the $cz_{\text{abs}} = 1586 \text{ km s}^{-1}$ metal-line system in the 3C 273 sight line $71 h_{70}^{-1} \text{ kpc}$ away. This dwarf poststarburst galaxy could be representative of a later stage in the evolution of the SBS 1122+594/IC 691 system. Once all of the H I in IC 691 has been exhausted via star formation and ejection it will develop a poststarburst spectrum and fade in luminosity as envisioned by Babul & Rees (1992) to the current brightness of the 3C 273 dwarf ($M_B = -13.9$) within $\sim 1 \text{ Gyr}$ after the H I is exhausted (Bruzual & Charlot 1993, 2003; Babul & Ferguson 1996). Meanwhile, the unbound wind will continue to propagate into the surrounding IGM and increase the distance that IC 691 has distributed metals.

On the other hand, more luminous galaxies appear to produce bound winds. Keeney et al. (2005) found that the nearby luminous ($0.5 L^*$) starburst galaxy NGC 3067 ($\text{SFR} \approx 1.4 M_{\odot} \text{ yr}^{-1}$) produces a bound wind along the 3C 232 sight line, which probes the halo of NGC 3067 near its minor axis and $11 h_{70}^{-1} \text{ kpc}$ from the plane. Similarly, Keeney et al. (2006) found that the Milky Way produces a bound wind toward two high-latitude AGN sight lines near $l = 0^{\circ}$ (Mrk 1383 and PKS 2005–489) that probe regions directly to the north and south of the Galactic Center at heights of up to 12.5 kpc. In both NGC 3067 and the Milky Way, the bound winds have the same spectral signature as high-velocity clouds and share many of their properties.

Statistical studies of QSO-absorber pairs in large samples of low- z Ly α +metal line

absorbers (e.g., Stocke et al. 2006b) also suggest that IGM metals are spread primarily by dwarf galaxies. For example, Tumlinson & Fang (2005) found that enriched regions of gas must extend ~ 1 Mpc from L^* galaxies to be due to $\geq L^*$ galaxy superwinds. Enrichment regions of 100–150 kpc are much more plausible based upon observed absorber-galaxy distances (Stocke et al. 2006b), but require that enrichment is due primarily to dwarf ($\lesssim 0.1 L^*$) galaxies (Tumlinson & Fang 2005). The SBS 1122+594/IC 691 system supports this conclusion.

IC 691 is not the only blue compact galaxy that shows evidence for an outflowing wind. The Fornax Cluster galaxy FCC 35 shows strong $H\alpha$ and [O III] emission and an unusual single-dish H I 21 cm profile in which a rotationally supported H I disk is superimposed with an irregularly shaped H I cloud with no optical counterpart (Putman et al. 1998). The disk and the cloud have roughly the same H I mass ($M_{\text{HI}} = 2.2 \times 10^8 M_{\odot}$) and overlap spatially but not in velocity, with the cloud blueshifted by $\sim 150 \text{ km s}^{-1}$ with respect to the systemic velocity of the disk. While the cloud has no velocity structure, the rotation curve of the disk indicates that it has a truncated mass distribution. Putman et al. (1998) suggest that the H I cloud is triggering the current burst of star formation in FCC 35, but by analogy with IC 691 the H I cloud could also be ejecta from the starburst wind of FCC 35, which would explain the truncated mass distribution of its disk. FCC 35 has an H I mass comparable to the galaxies with the lowest gas masses and smallest gas depletion timescales in the Pisano et al. (2001) sample of nearby blue compact galaxies. These low-mass galaxies may be undergoing their last star formation event and will likely fade in luminosity as envisioned by Babul & Rees (1992) once their current star formation ceases (Pisano et al. 2001).

Collectively, these results imply that starburst winds escape more easily from dwarf starburst galaxies than their more massive counterparts. This is to be expected since Meurer et al. (1997) found a maximum areal SFR of $\sim 45 M_{\odot} \text{ kpc}^{-2} \text{ yr}^{-1}$ for starbursts of all luminosities and Martin (1999) found that the temperature of starburst winds is nearly constant as a function of galaxy mass, both of which imply that the strength of a starburst wind is independent of galaxy size. Thus, there is growing evidence that the metals and energy expelled by massive galaxies are retained in their bound halos and the weaker but more numerous dwarfs are primarily responsible for enriching the IGM.

We have argued that an outflowing unbound starburst wind from IC 691 is the best model for explaining the origin of the metal-line absorber in the spectrum of SBS 1122+594 due to: (1) the proximity of the QSO sight line to the galaxy’s minor axis, (2) the on-going star formation in IC 691, (3) the energetic ability of the current IC 691 starburst to eject $\sim 10^7 M_{\odot}$ of material to the observed wind velocity after escaping the galaxy’s gravitational potential well, and (4) the consistent subsolar metallicities derived for IC 691

and the metal-line absorber. However, other plausible models for the absorber origin exist. In particular, we cannot rule out the possibility that the absorber is caused by diffuse tidal debris from the recent interaction of IC 691 and SDSS J1126+593, although the observed geometry of the H I 21 cm emitting gas does not obviously support this hypothesis. Future observations of SBS 1122+594 as well as fainter AGN near IC 691 with the Cosmic Origins Spectrograph (COS) would allow us to distinguish between these models and sensitively search for absorption in other ions at $cz \sim 1110 \text{ km s}^{-1}$.

We acknowledge support from NASA HST General Observer grant GO-09874 to the University of Chicago, and grants GO-09506 and GO-06593 to the University of Colorado. B. A. K. acknowledges support from NASA Graduate Student Researchers Program grant NGT5-154. J. L. R. acknowledges support from NSF grant AST-0302049. J. T. gratefully acknowledges the generous support of the Gilbert and Jaylee Mead Family Foundation through the Yale Department of Physics. We also thank Mark Giroux for use of his photoionization models.

This work is based on observations made with the NASA/ESA *Hubble Space Telescope* (HST), the Apache Point Observatory (APO) 3.5-meter telescope, the Kitt Peak National Observatory (KPNO) 2.1-meter telescope, and the Very Large Array (VLA) of the National Radio Astronomy Observatory (NRAO). The HST data were obtained at the Space Telescope Science Institute, which is operated by the Association of Universities for Research in Astronomy, Inc., under NASA contract NAS5-26555. The APO 3.5-m telescope is owned and operated by the Astrophysical Research Consortium. KPNO is operated by the Association of Universities for Research in Astronomy, Inc. (AURA) under cooperative agreement with the National Science Foundation. The NRAO is a facility of the National Science Foundation operated under cooperative agreement by Associated Universities, Inc. This research has also made use of the NASA/IPAC Extragalactic Database (NED) and the Sloan Digital Sky Survey (SDSS). NED is operated by the Jet Propulsion Laboratory, California Institute of Technology, under contract with the National Aeronautics and Space Administration,

A. Appendix

The full STIS G140L snapshot spectrum of SBS 1122+594 is displayed in Figure 8. This spectrum shows a $\sim 30\%$ continuum decrement blueward of $\sim 1435 \text{ \AA}$, which suggests the presence of a partial Lyman limit system (LLS) at $z \sim 0.58$. A search for other absorption lines at this redshift revealed $\text{Ly}\beta$, C II/C II*, and O I absorption at $z = 0.583$. The apparent optical depth (AOD; Savage & Sembach 1991) of the $\text{Ly}\beta$ line places a lower

limit on the H I column density of the LLS of $N_{\text{HI}} > 10^{15.4} \text{ cm}^{-2}$. LLSs have column densities of $N_{\text{HI}} = 10^{17.3-20.3} \text{ cm}^{-2}$ and an optical depth at the Lyman limit of $\tau_{\text{LL}} \gtrsim 1$. The $28 \pm 13\%$ continuum decrement in our spectrum of SBS 1122+594 implies an optical depth at the Lyman limit of $\tau_{\text{LL}} = 0.3 \pm 0.2$, which requires an H I column density of $N_{\text{HI}} = (5 \pm 3) \times 10^{16} \text{ cm}^{-2}$.

The positions of Galactic lines in Figure 8 are indicated with tickmarks below the spectrum and the positions of intergalactic absorption lines are indicated with tickmarks above the spectrum. The Ly α and C IV lines at $cz_{\text{abs}} = 1110 \pm 30 \text{ km s}^{-1}$ (see Fig. 1) are shown with dotted tickmarks, lines associated with the LLS at $z = 0.583$ are shown with dashed tickmarks, and intergalactic Ly α lines at other redshifts are shown with solid tickmarks. We have not searched for associated metal lines at the redshifts of the Ly α absorbers indicated with solid tickmarks. The broad feature at $\sim 1460 \text{ \AA}$ is likely intrinsic O IV 787 \AA emission at $z = 0.852$. The signal-to-noise ratio of the spectrum ranges from ~ 10 per resolution element near Galactic Ly α to ~ 5 per resolution element near Galactic Al II, which corresponds to 3σ equivalent width limits of 360 m \AA and 510 m \AA , respectively.

Neither the SDSS spectrum of SBS 1122+594 nor a DIS spectrum taken on 2003 May 2 show Mg II absorption at $z = 0.58$ with an equivalent width $\gtrsim 50 \text{ m\AA}$. Luminous ($L > 0.1-0.3 L^*$) galaxies are typically found within a projected distance of $50 h_{70}^{-1} \text{ kpc}$ of LLSs with strong Mg II absorption (Steidel 1995, 1998). Our R-band image of IC 691 (see § 2.2) does not show a $L \gtrsim 0.3 L^*$ ($m_R \lesssim 21.0$; Brown et al. 2001) galaxy within $50 h_{70}^{-1} \text{ kpc}$ ($6''$ at $z = 0.58$) of SBS 1122+594 that could be responsible for this LLS (the SDSS plates show no galaxy within $50 h_{70}^{-1} \text{ kpc}$ of SBS 1122+594 with $L \gtrsim 0.7 L^*$ in i' -band or $L \gtrsim 3 L^*$ in z' -band; Blanton et al. 2001). Our B-band and near-infrared images of IC 691 cannot be used to search for the galaxy responsible for this LLS because they do not have a large enough field of view to cover the SBS 1122+594 sight line. Since the LLS seen in the STIS spectrum of SBS 1122+594 does not produce a strong Mg II absorber, it is not surprising that our images do not show a luminous galaxy within a projected distance of $50 h_{70}^{-1} \text{ kpc}$ from the sight line.

REFERENCES

- Abazajian, K. et al. 2005, AJ, 129, 1755
- Adelberger, K., Steidel, C. C., Shapley, A. E., & Pettini, M. 2003, ApJ, 584, 45
- Aracil, B., Tripp, T. M., Bowen, D. V., Prochaska, J. X., Chen, H.-W., & Frye, B. L. 2006, MNRAS, 367, 139

- Babul, A. & Rees, M. J. 1992, MNRAS, 255, 346
- Babul, A. & Ferguson, H. C. 1996, ApJ, 458, 100
- Begum, A., Chengalur, J. N., & Karachentsev, I. D. 2005, A&A, 443, L1
- Blanton, M. R. et al. 2001, AJ, 121, 2358
- Brown, W. R., Geller, M. J., Fabricant, D. G., & Kurtz, M. J. 2001, AJ, 122, 714
- Bruzual, G. A. & Charlot, S. 1993, ApJ, 405, 538
- Bruzual, G. & Charlot, S. 2003, MNRAS, 344, 1000
- Charlton, J. C., Churchill, C. W., Ding, J., Zonak, S., Bond, N., & Rigby, J. R. 2002, in *Extragalactic Gas at Low Redshift*, ed. J. Mulchaey & J. Stocke (San Francisco: ASP), 122
- Cioffi, D. F. & Shull, J. M. 1991, ApJ, 367, 96
- Danforth, C. W. & Shull, J. M. 2005, ApJ, 624, 555
- Danforth, C. W., Shull, J. M., Rosenberg, J. L., & Stocke, J. T. 2006, ApJ, 640, 716
- de Vaucouleurs, G. 1948, *Ann. d’Astrophys.*, 11, 247
- Filippenko, A. V. & Sargent, W. L. W. 1992, AJ, 103, 28
- Heckman, T. M., Armus, L., & Miley, G. K. 1990, ApJS, 74, 833
- Heckman, T. M., Lehnert, M. D., Strickland, D. K., & Armus, L. 2000, ApJS, 129, 493
- Heckman, T. M., Sembach, K. R., Meurer, G. R., Strickland, D. K., Martin, C. L., Calzetti, D., & Leitherer, C. 2001, ApJ, 554, 1021
- Hibbard, J. & van Gorkom, J. H. 1996, AJ, 111, 655
- Impey, C. D., Petry, C. E., & Flint, K. P. 1999, ApJ, 524, 536
- Keeney, B. A., Momjian, E., Stocke, J. T., Carilli, C. L., & Tumlinson, J. 2005, ApJ, 622, 267
- Keeney, B. A., Danforth, C. W., Stocke, J. T., Penton, S. V., Shull, J. M., & Sembach, K. R. 2006, ApJ, 646, 951
- Kennicutt, R. C. 1983, ApJ, 272, 54

- Kennicutt, R. C., Jr. 1998, *ARA&A*, 36, 189
- Koo, B.-C. & McKee, C. F. 1992a, *ApJ*, 388, 93
- Koo, B.-C. & McKee, C. F. 1992b, *ApJ*, 388, 103
- Marcolini, A., Strickland, D. K., D’Ercole, A., Heckman, T. M., & Hoopes, C. G. 2005, *MNRAS*, 362, 626
- Marlowe, A. T., Heckman, T. M., Wyse, R. F. G., & Schommer, R. 1995, *ApJ*, 438, 563
- Martin, C. L. 1998, *ApJ*, 506, 222
- Martin, C. L. 1999, *ApJ*, 513, 156
- Martin, C. L. 2003, in *The IGM/Galaxy Connection*, ed. J. Rosenberg & M. Putman (Dordrecht: Kluwer), 205
- Martin, C. L. 2005, *ApJ*, 621, 227
- Martin, C. L. 2006, *ApJ*, in press (astro-ph/0604173)
- Martin, C. L., Kobulnicky, H. A., & Heckman, T. M. 2002, *ApJ*, 574, 663
- Marzke, R. O., Huchra, J. P., & Geller, M. J. 1994, *ApJ*, 428, 43
- Mateo, M. L. 1998, *ARA&A*, 36, 435
- Meurer, G. R. et al. 1997, *ApJ*, 114, 54
- Morris, S. L., Weymann, R. J., Dressler, A., McCarthy, P. J., Smith, B. A., Terrile, R. J., Giovanelli, R., & Irwin, M. 1993, *ApJ*, 419, 524
- Morton, D. C. 2003, *ApJS*, 149, 205
- Norman, C. A., Bowen, D. V., Heckman, T., Blades, C., & Danly, L. 1996, *ApJ*, 472, 73
- Oey, M. S. & Shields, J. C. 2000 *ApJ*, 539, 687
- Oey, M. S., Dopita, M. A., Shields, J. C. & Smith, R. C. 2000, *ApJS*, 128, 511
- Ott, J., Martin, C. L., & Walter, F. 2003, *ApJ*, 594, 776
- Penton, S. V., Stocke, J. T., & Shull, J. M. 2002, *ApJ*, 565, 720
- Penton, S. V., Stocke, J. T., & Shull, J. M. 2004, *ApJS*, 152, 29

- Pettini, M., Shapley, A. E., Steidel, C. C., Cuby, J.-G., Dickinson, M., Moorwood, A. F. M., Adelberger, K. L., & Giavalisco, M. 2001, *ApJ*, 554, 981
- Pettini, M., Rix, S. A., Steidel, C. C., Adelberger, K. L., Hunt, M. P., & Shapley, A. E. 2002, *ApJ*, 569, 742
- Pisano, D. J., Kobulnicky, H. A., Guzmán, R., Gallego, J., & Bershad, M. A. 2001, *AJ*, 112, 1194
- Prochaska, J. X., Chen, H.-W., Howk, J. C., Weiner, B. J., & Mulchaey, J. 2004, *ApJ*, 617, 718
- Putman, M. E., Bureau, M., Mould, J. R., Staveley-Smith, L., & Freeman, K. C. 1998, *AJ*, 115, 2345
- Roberts, M. S. & Haynes, M. P. 1994, *ARA&A*, 32, 115
- Rosenberg, J. L., Ganguly, R., Giroux, M. L., & Stocke, J. T. 2003, *ApJ*, 591, 677
- Rupke, D. S., Veilleux, S., & Sanders, D. B. 2005a, *ApJS*, 160, 87
- Rupke, D. S., Veilleux, S., & Sanders, D. B. 2005b, *ApJS*, 160, 115
- Savage, B. D. & Sembach, K. R. 1991, *ApJ*, 379, 245
- Schwartz, C. M. & Martin, C. L. 2004, *ApJ*, 610, 201
- Sembach, K. R., Howk, J. C., Savage, B. D., Shull, J. M., & Oegerle, W. R. 2001, *ApJ*, 561, 573
- Shull, J. M., Penton, S. V., Stocke, J. T., Giroux, M. L., van Gorkom, J. H., Lee, Y. H., & Carilli, C. 1998, *AJ*, 116, 2094
- Shull, J. M., Tumlinson, J., & Giroux, M. L. 2003, *ApJ*, 594, L107
- Staveley-Smith, L., Davies, R. D., & Kinman, T. D. 1992, *MNRAS*, 258, 334
- Steidel, C. C. 1995, in *QSO Absorption Lines*, ed. G. Meylan (Berlin: Springer), 139
- Steidel, C. C. 1998, in *ASP Conf. Ser. 136, Galactic Halos*, ed. D. Zaritsky (San Francisco: ASP), 167
- Steidel, C. C., Giavalisco, M., Dickinson, M., & Adelberger, K. L. 1996a, *AJ*, 112, 352

- Steidel, C. C., Giavalisco, M., Pettini, M., Dickinson, M., & Adelberger, K. L. 1996b, *ApJ*, 462, L17
- Steidel, C. C., Adelberger, K. L., Giavalisco, M., Dickinson, M., & Pettini, M. 1999, *ApJ*, 519, 1
- Steidel, C. C., Pettini, M., & Adelberger, K. L. 2001, *ApJ*, 546, 665
- Stocke, J. T., Keeney, B. A., McLin, K. M., Rosenberg, J. L., Weymann, R. J., & Giroux, M. L. 2004, *ApJ*, 609, 94
- Stocke, J. T., Shull, J. M., & Penton, S. V. 2006a, in *Planets to Cosmology*, ed. S. Casertano & M. Lirio (Cambridge: Cambridge Univ. Press), in press (astro-ph/0407352)
- Stocke, J. T., Penton, S. V., Danforth, C. W., Shull, J. M., Tumlinson, J., & McLin, K. M. 2006b, *ApJ*, 641, 217
- Strickland, D. K., Heckman, T. M., Colbert, E. J. M., Hoopes, C. G., & Weaver, K. A. 2004, *ApJ*, 606, 829
- Suchkov, A. A., Berman, V. G., Heckman, T. M., & Balsara, D. S. 1996, *ApJ*, 463, 528
- Tripp, T. M., Lu, L., & Savage, B. D. 1998, *ApJ*, 508, 200
- Tripp, T. M. et al. 2002, *ApJ*, 575, 697
- Tumlinson, J. & Fang, T. 2005, *ApJ*, 623, L97
- Tumlinson, J., Shull, J. M., Giroux, M. L., & Stocke, J. T. 2005, *ApJ*, 620, 95
- Veilleux, S., Cecil, G., Bland-Hawthorn, J., Tully, R. B., Filippenko, A. V., & Sargent, W. L. W. 1994, *ApJ*, 433, 48
- Veilleux, S., Cecil, G., & Bland-Hawthorn, J. 2005, *ARA&A*, 43, 769
- Watson, M. G., Stanger, V., & Griffiths, R. E. 1984, *ApJ*, 286, 144
- York, D. G. et al. 2000, *AJ*, 120, 1579
- York, D. G. et al. 2006, *MNRAS*, 367, 945

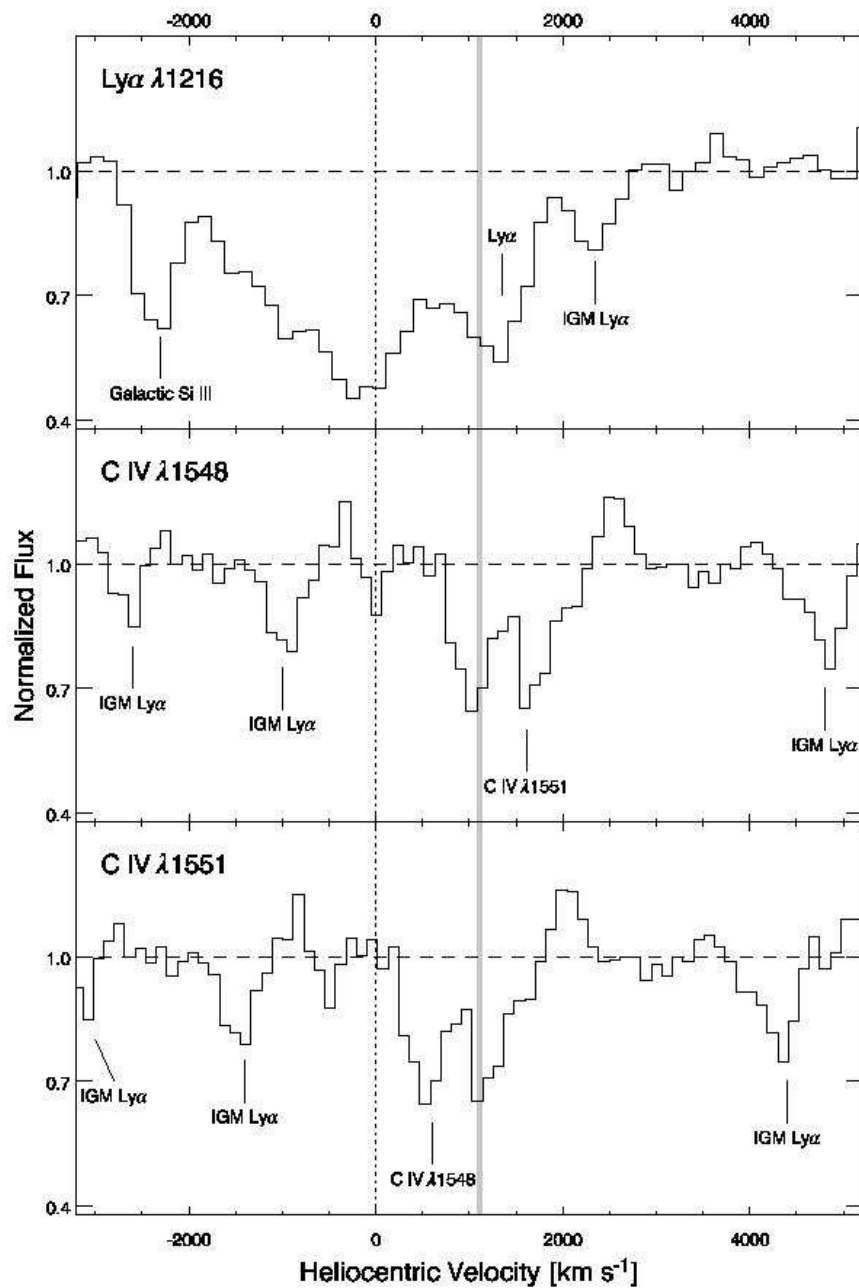


Fig. 1.— $\text{Ly}\alpha$ (top panel) and C IV (middle and bottom panels) absorption features from the HST/STIS snapshot spectrum of SBS 1122+594. The best-fit absorber velocity of $cz_{\text{abs}} = 1110 \pm 30 \text{ km s}^{-1}$ (determined from the C IV lines only) is indicated by the vertical gray bar. Features centered near the dotted vertical line at $v = 0$ are Galactic and all other absorption features have been identified and labelled.

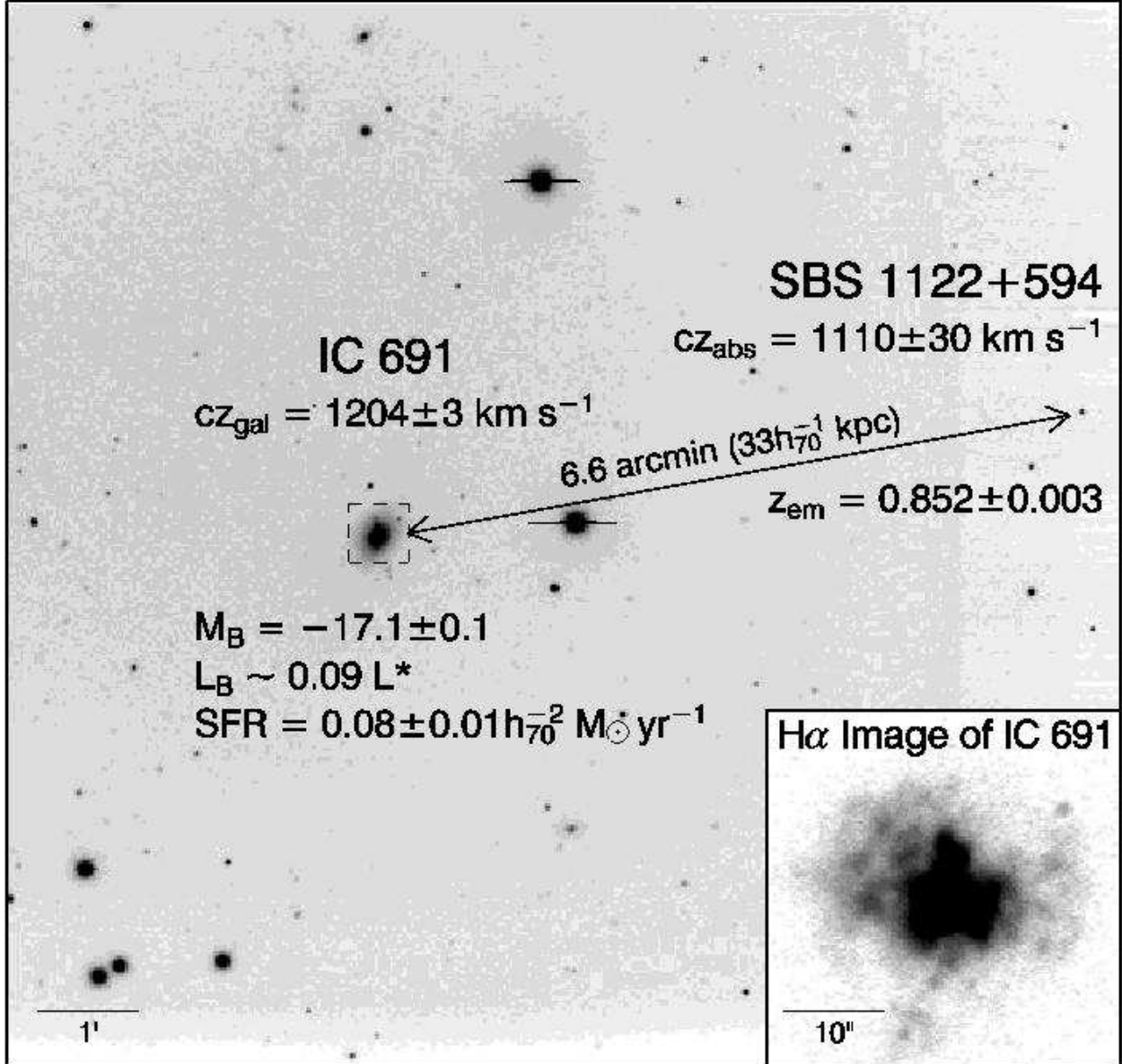


Fig. 2.— R-band mosaic of the QSO/galaxy pair SBS 1122+594/IC 691 taken with the KPNO 2.1-m telescope. The inset, whose approximate boundary is marked by the dashed box in the mosaic, shows a pure H α image of IC 691. The seeing in the mosaic is 1".8 and the seeing in the inset is 1".5.

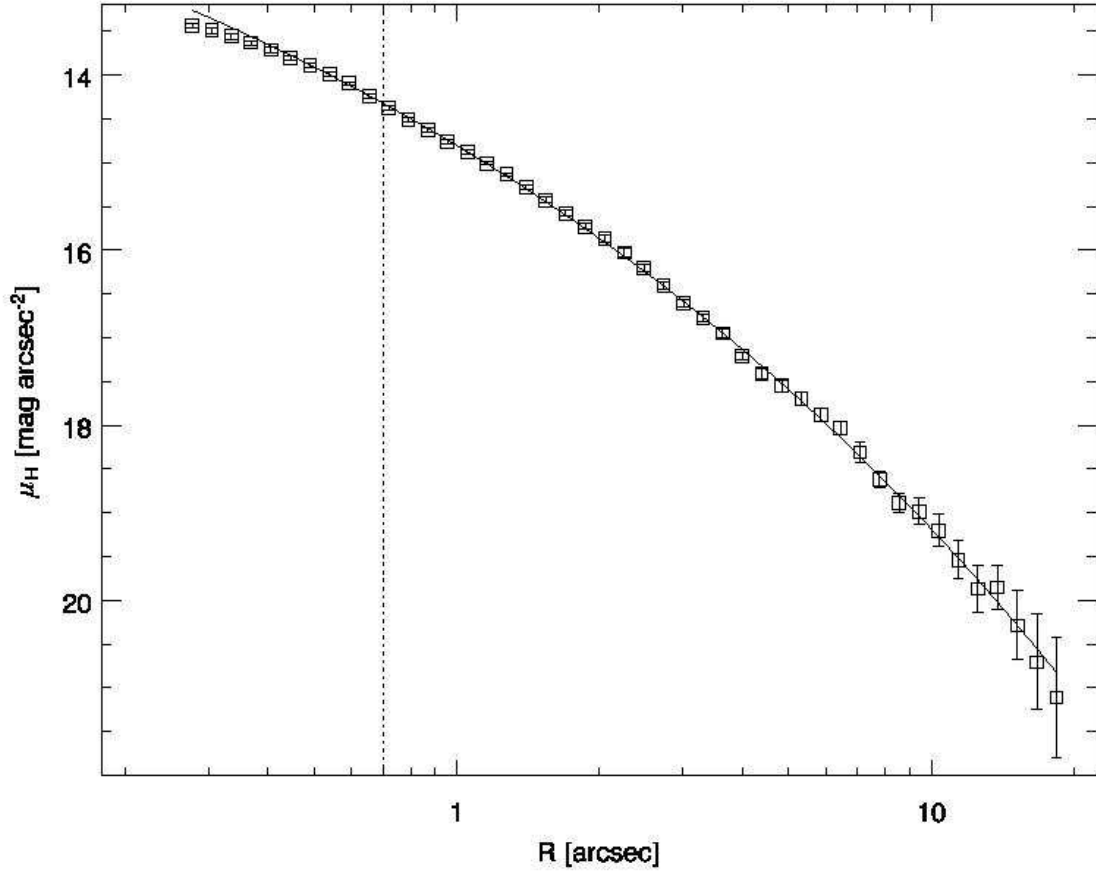


Fig. 3.— Surface brightness profile of IC 691 in H-band. The best-fit (reduced $\chi^2 = 0.6$ for $R \geq 0''.7$) de Vaucouleurs (1948) $R^{1/4}$ profile, which has an effective radius of $r_e = 400 \pm 10 h_{70}^{-1}$ pc and a fiducial surface brightness of $\mu_H(r_e) = 17.49 \pm 0.07$ mag arcsec⁻², is overlaid with a solid line. The seeing of $0''.7$ is indicated by a vertical dotted line.

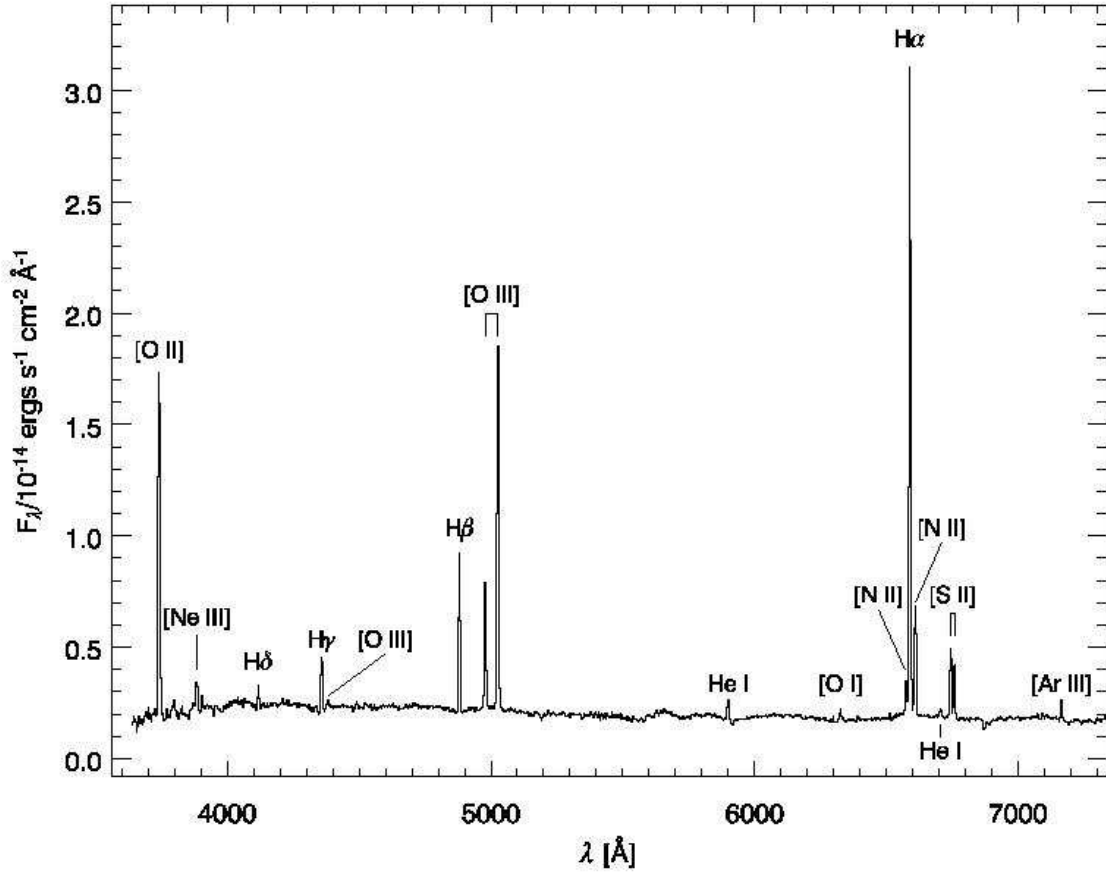


Fig. 4.— Optical spectrum of IC 691 taken with the ARC 3.5-m telescope at Apache Point Observatory. This spectrum was acquired through a $1''.5$ slit rotated to a position angle of 90° and was extracted using a $12''$ wide aperture. All of the emission lines listed in Table 1 are labelled.

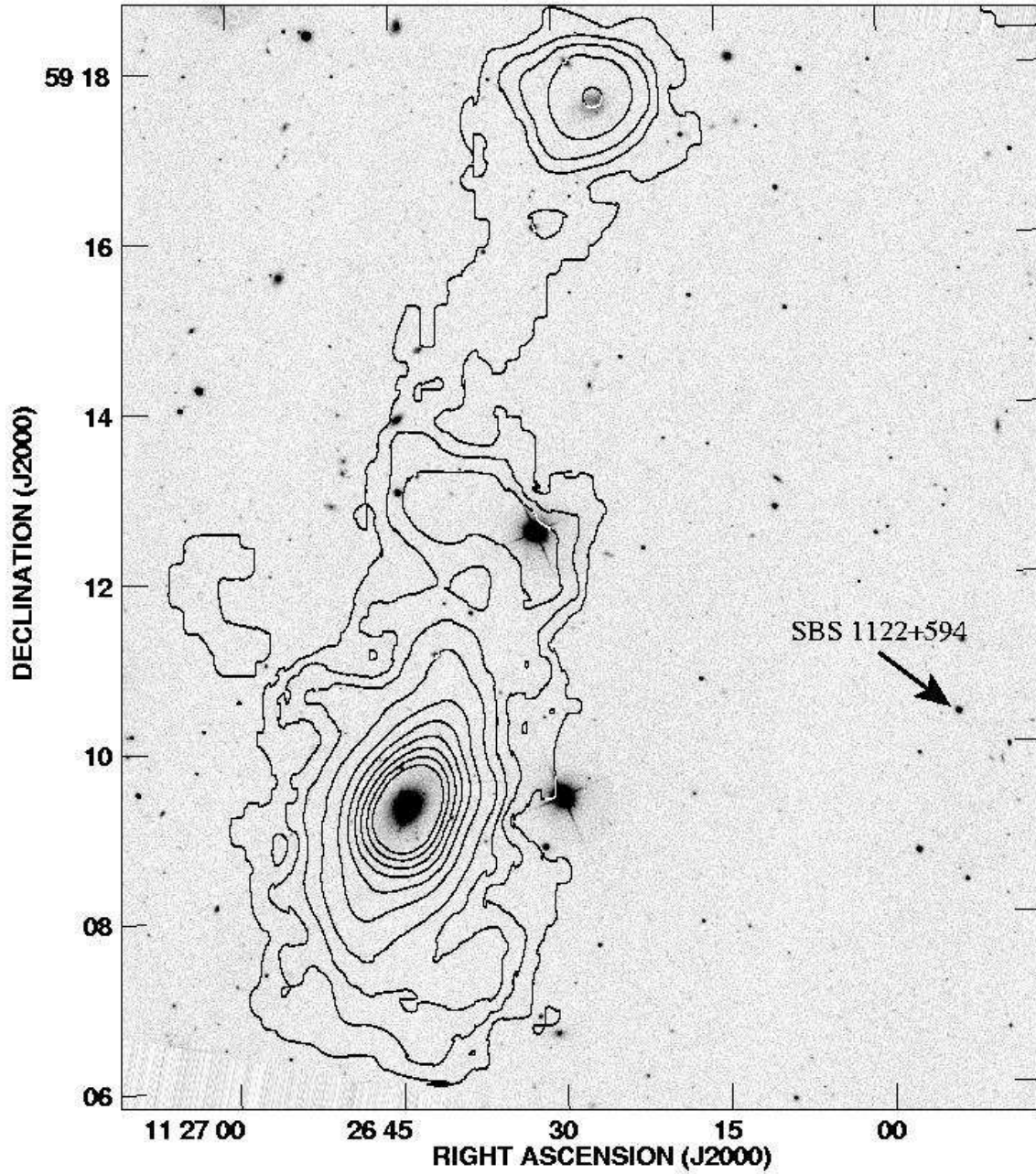


Fig. 5.— H I 21 cm intensity contours for IC 691 overlaid on a SDSS g' -band image. Contour levels are at $1.78, 8.92, 17.8, 35.7, 71.4, 107, 143, 178, 214,$ and 250×10^{18} atoms cm^{-2} . IC 691 is interacting with SDSS J1126+593, an LSB galaxy to the north. The position of SBS 1122+594 is also labelled.

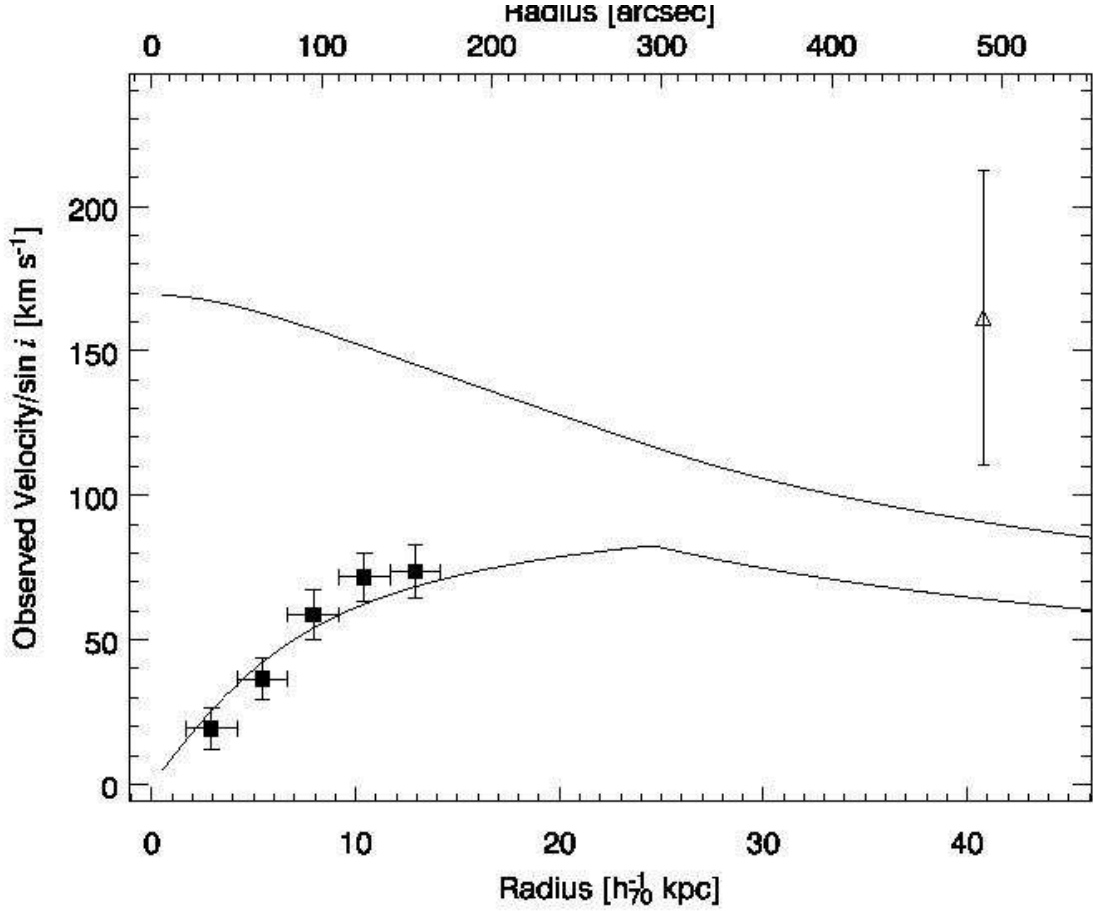


Fig. 6.— Rotation curve of IC 691 with a truncated isothermal halo model overlaid. The model assumes that the rotation curve is flat to a radius of $24.6 h_{70}^{-1}$ kpc ($295''$) and has a best-fit central density of $\rho_0 = 0.005 \pm 0.002 M_{\odot} \text{pc}^{-3}$ and a core radius of $6 \pm 2 h_{70}^{-1}$ kpc. The solid line above the data points indicates the escape velocity as a function of radius predicted by the best-fit model. The data point with the open triangle symbol shows the derived wind velocity and absorber location (§ 4.2). All quantities assume that IC 691 is at an inclination of $i = 54^{\circ}$.

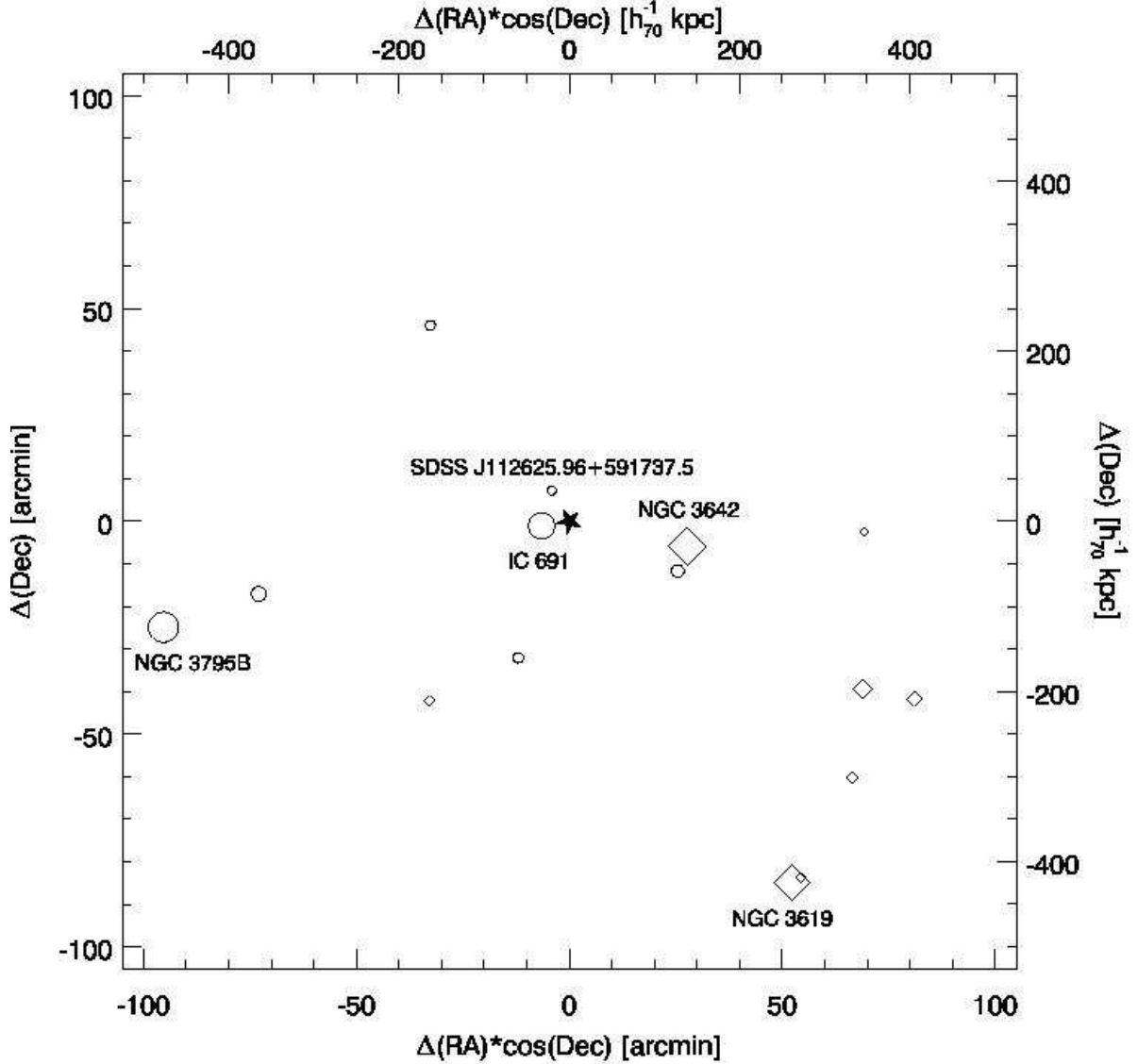


Fig. 7.— All galaxies with $cz < 1600 \text{ km s}^{-1}$ that are within $500 h_{70}^{-1} \text{ kpc}$ of SBS 1122+594 ($100'$ at $cz = 1200 \text{ km s}^{-1}$), as compiled by SDSS and NED. All positions are relative to SBS 1122+594 ($\text{RA} = 11^{\text{h}} 25^{\text{m}} 53.8^{\text{s}}$, $\text{Dec} = 59^{\circ} 10' 22''$), which is represented by the filled star symbol in the center of the plot. Circles represent galaxies with $cz < 1300 \text{ km s}^{-1}$ and diamonds represent galaxies with $cz = 1300\text{--}1600 \text{ km s}^{-1}$. Symbol size is proportional to SDSS r' -band luminosity, with a factor of 2 increase in symbol size equivalent to a factor of 10 increase in luminosity. The galaxies discussed in § 3 are also labelled.

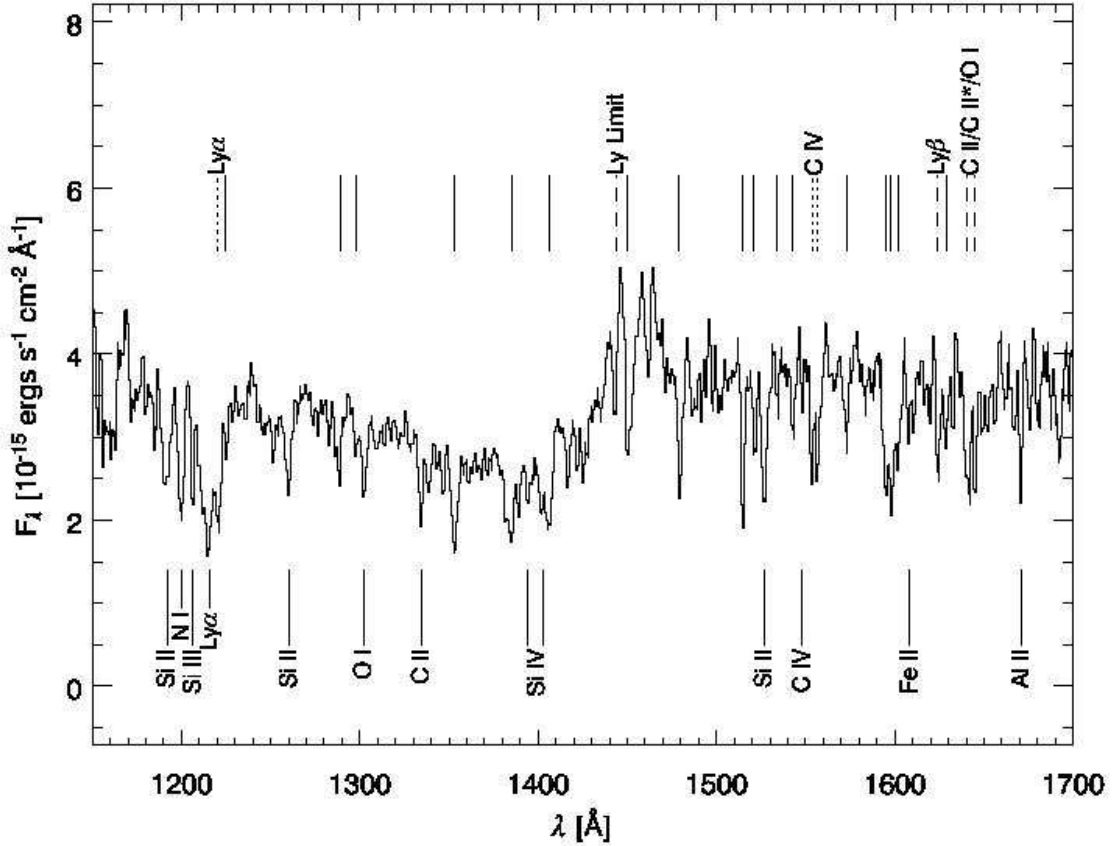


Fig. 8.— The full STIS G140L snapshot spectrum of SBS 1122+594. The positions of Galactic lines are indicated with tickmarks below the spectrum and the positions of intergalactic absorption lines are indicated with tickmarks above the spectrum. The Ly α and C IV lines at $cz_{\text{abs}} = 1110 \pm 30$ km s^{-1} (see Fig. 1) are shown with dotted tickmarks, lines associated with the LLS at $z = 0.583$ are shown with dashed tickmarks, and intergalactic Ly α lines at other redshifts are shown with solid tickmarks. The signal-to-noise ratio of the spectrum ranges from ~ 10 per resolution element near Galactic Ly α to ~ 5 per resolution element near Galactic Al II.

Table 1. IC 691 Optical Emission Line Equivalent Widths

Line Identification	W_λ (\AA)
[O II] 3727 \AA	68 ± 5
[Ne III] 3869 \AA	4 ± 1
H δ	2.2 ± 0.4
H γ	7.4 ± 0.5
[O III] 4363 \AA	1.2 ± 0.2
H β	28 ± 1
[O III] 4959 \AA	23 ± 1
[O III] 5007 \AA	66 ± 2
He I 5876 \AA	3 ± 1
[O I] 6300 \AA	2.3 ± 0.6
[N II] 6548 \AA	7.0 ± 0.8
H α	117 ± 4
[N II] 6584 \AA	20 ± 1
He I 6678 \AA	1.6 ± 0.3
[S II] 6717 \AA	13.0 ± 0.6
[S II] 6731 \AA	10.4 ± 0.6
[Ar III] 7136 \AA	4.1 ± 0.8